applied sciences

MDPI

Article

A Novel Type of Wall-Climbing Robot with a Gear Transmission System Arm and Adhere Mechanism Inspired by Cicada and Gecko

Shiyuan Bian [1,2], Feng Xu [1,2], Yuliang Wei [1,2] and Deyi Kong [1,3,*]

[1] Institute of Intelligent Machines, Hefei Institutes of Physical Science, Chinese Academy of Sciences, Hefei 230031, China; sybian@iim.ac.cn (S.B.); xf1992@mail.ustc.edu.cn (F.X.); wyl1010@mail.ustc.edu.cn (Y.W.)
[2] Science Island Branch of Graduate School, University of Science and Technology of China, Hefei 230009, China
[3] Innovation Academy for Seed Design, Chinese Academy of Sciences, Sanya 572024, China
* Correspondence: kongdy@iim.ac.cn

Abstract: To support the inspections of different contact walls (rough and smooth), a novel type of wall-climbing robot was proposed. Its design embodied a new gear transmission system arm and an adherence mechanism inspired by cicadas and geckos. The actuating structure consisted of a five-bar link and a gear transmission for the arm stretching, which was driven by the servos. The linkers and gears formed the palm of this robot for climbing on a line. Moreover, the robot's adherence method for the rough surfaces used bionic spine materials inspired by the cicada. For smooth surface, a bionic adhesion material was proposed inspired by the gecko. To assess the adherence mechanism of the cicada and gecko, the electron microscope images of the palm of the cicada and gecko were obtained by an electron microscope. The 3D printing technology and photolithography technology were utilized to manufacture the robot's structures. The adherence force experiments demonstrated the bionic spines and bionic materials achieved good climbing on cloth, stones, and glass surfaces. Furthermore, a new gait for the robot was designed to ensure its stability. The dynamic characteristics of the robot's gear transmission were obtained.

Keywords: wall-climbing robot; gear transmission; bionic spine; electron microscope images; 3D printing technology

Citation: Bian, S.; Xu, F.; Wei, Y.; Kong, D. A Novel Type of Wall-Climbing Robot with a Gear Transmission System Arm and Adhere Mechanism Inspired by Cicada and Gecko. *Appl. Sci.* **2021**, *11*, 4137. https://doi.org/10.3390/app11094137

Academic Editor: TaeWon Seo

Received: 12 March 2021
Accepted: 28 April 2021
Published: 30 April 2021

1. Introduction

Researchers investigating wall-climbing robots looked to nature for inspiration. Around the gecko, researchers studied the gecko's toe and crawling approach to propose some wall-climbing robots. On the basis of numerous studies on the gecko [1–6], the gecko's adhesion mechanism was proposed, and the relevant wall-climbing robots inspired by the gecko were investigated. Metin et al. [7] assessed a four-legged wall-climbing robot with an elastomer adhesive pad to climb a sloped surface. A novel robot [8] was presented with a shape memory alloy actuator to drive its climbing. A microfiber with an angled mushroom tips [9] array inspired by gecko was manufactured for a novel wall-climbing robot, Waalbot [10,11]. These studies applied the special structure array inspired by the gecko to the wall-climbing robot. Cutkosky et al. [12–15] learned from the gecko's pad and body structure to present a gecko-like, wall-climbing robot. A bionic pad of this robot consisted of a microfiber array and four-legged locomotion. The tail was inspired by the gecko's toe and the gecko's climbing gait. Dai et al. [16] proposed a novel wall-climbing robot with a biomimetic gait inspired by the gecko, which adjusted the posture of the robot's foot to stably adhere to the wall. Mei et al. [17,18] assessed a tank-like, wall-climbing robot with gecko-inspired material on the caterpillar band. This robot climbed on a vertical surface, on the ceiling, or travelled from the vertical surface to the ceiling.

In another line of research, a series of studies were presented on wall-climbing robots inspired by animals with claws for traversing rough surfaces. Dai et al. [19] proposed a model of claws' adherence on rough surfaces and investigated the relation of the dimensions of the claws with respect to the particles. Cutkosky et al. [20–22] presented a six-legged, wall-climbing robot with alternating tripod gait for climbing a wall with stability. Saunders et al. [23] proposed a RiSE robot with six legs and flexible spines inspired by insects. The robot climbed a 90° tree in addition to carpeted and cork covered stucco surfaces in the quasi-static regime. Then, the foot of this robot was improved to climb on the wall with stability. A new type of the wall-climbing robot [24] was assessed and demonstrated better performance. An improved wall-climbing robot [25] was proposed with better stability and faster movement. Based on the results presented by Goldman et al. [26] on the behaviors of the cockroach, Clark et al. [27–30] proposed a bionic, double-legged wall-climbing robot for rough surfaces. Furthermore, quadrupedal wall-climbing robots [31–33] were proposed with a lateral leg spring model. Liu [34] proposed a wheeled wall-climbing robot with bionic feet inspired by Serica orientalis Motschulsky; it was capable of climbing across the transition from horizontal to vertical surfaces. Then, a novel, tracked, wall-climbing robot with bio-inspired spine feet was presented for rough surface [35].

It can be seen from the literature that the wall-climbing robots studied by many researchers only aim at smooth or rough surfaces and rarely prepare wall-climbing robots that adapt to both smooth and rough surfaces. This paper proposes a novel type of wall-climbing robot with a gear transmission system arm for climbing on the smooth and rough surfaces that absorbs the adhesion characteristics of gecko and cicada. The novel actuating structure consisted of a five-bar link, gear transmission system, and drive source servos. The dynamic characteristics of the gear transmission of the robot were obtained by a numerical model. In the transmission system, the driving gear was driven by the servos, and the two driven gears were fixed with the links. In this approach, inspired by the cicada and gecko, the palm of the robot conformed to the line when climbing. Moreover, the bionic spine adherence materials and gecko-inspired materials were used to traverse rough surfaces and smooth surfaces. The robots' bodies were manufactured by using the 3D printing technology with resin. The adherence force experiments of the bionic spines and gecko-inspired materials were achieved on the rough and smooth surfaces. Finally, a new gait of the robot was designed to ensure the robot's climbing stability. The experiments of the robot climbing on the different walls are presented at the end. Based on the study of the bionic hooks and the materials bio-inspired by gecko, this robot, which can adapt to rough and smooth wall surfaces, was put forward innovatively.

2. Modeling of Wall-Climbing Robot

The cicada and gecko can climb on walls because of their feet with special microstructures. These microstructures give support for adhesion force for the cicada and gecko to adhere to a tree. This special adhesion ability was adopted in this robot for crawling on the wall with stability.

2.1. Robot Description

Figure 1a presents a novel, wall-climbing robot whose body was inspired by a gecko, with a gear transmission system arm. The robot included a head, a main body fixed on the control element and power module, feet driven by a gear transmission fixed on a five-bar link mechanism, and tail for supporting the robot climbing on a wall. The tail was connected to the body by a torsional ring, which provided a support force to the robot during climb. The five-bar link is presented in Figure 1b. The driving wheel is gear 1; gear 2 and gear 3 are the driven wheels. The link 1 and link 4 were fixed on gear 2 and gear 3, respectively. The four links (link 1, link 2, link 3, link 4) were connected by small bearings. The driving wheel gear 1 meshed with gear 2 and gear 3 at the same time on the supporting part to keep the palm moving on the line. Figure 1c presents the prototype

of this robot designed by 3D printing technology with resin material. The bio-inspired hooks were assembled to the palm. The length of a single hook was 18 mm. The length of the body was 474 mm (including tail), and the body width was 315 mm (including the four legs).

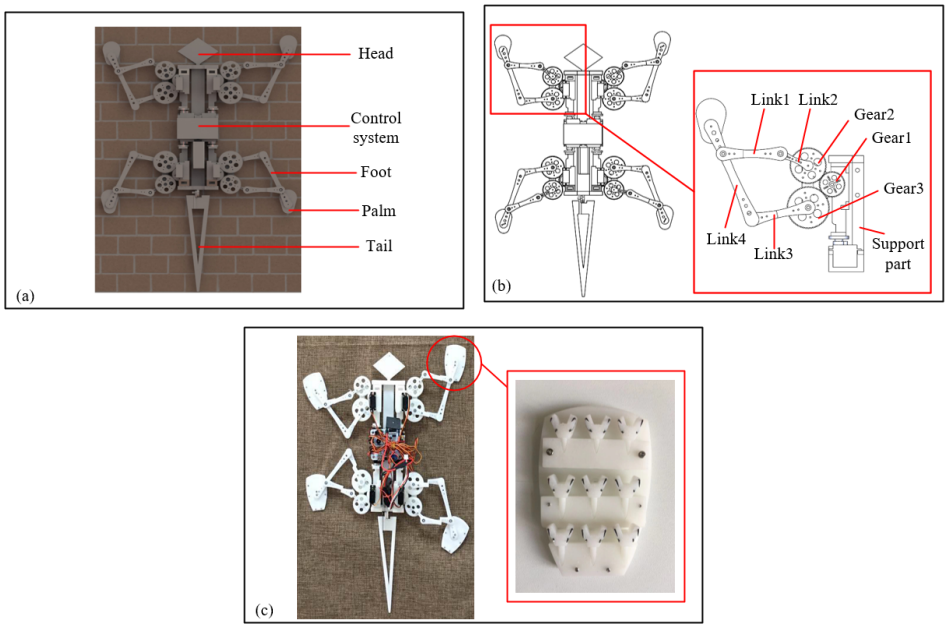

Figure 1. The design of a bio-inspired, wall-climbing robot: (**a**) the components of this robot, (**b**) the mechanism structure of the foot on the robot, (**c**) the prototype of this robot.

2.2. Statics' Analysis

This robot, adhering on the wall by its four palms and the tail, is shown in Figure 2a. The palms and tail provided the force to prevent the robot from falling down and capsizing.

$$\begin{cases} \sum_{i=1}^{4} F_{iy} + F_{ty} = G \\ \sum_{i=1}^{4} F_{ix} l_i + F_{tx} l_t = Gh \end{cases} \quad (1)$$

Here, G is the weight of the robot, F_{iy} (i = 1, 2, 3, 4) is the component of the force of the palms on the vertical destination, and F_{ty} is the component of the force of the tail on the vertical destination.

Figure 2b shows the force analysis of the robot's palm lift from B1 to B2 away from the surface by the servo located horizontally. The servo provides the momentum to lift the palm away from the surface, and the force analysis is shown as:

$$(G_p + F_a) L_p \cos(\theta_p) = M_p \quad (2)$$

Here, G_p represents the palm's weight, F_a is the adherence force of the palm lift from the surface by the bionic adherence material, L_p represents the length of the center position of the palm to the rotation center of the servo position O, θ_p is the angle the palm rotates from the position B1 to B2, and M_p is the momentum of the servo on the part.

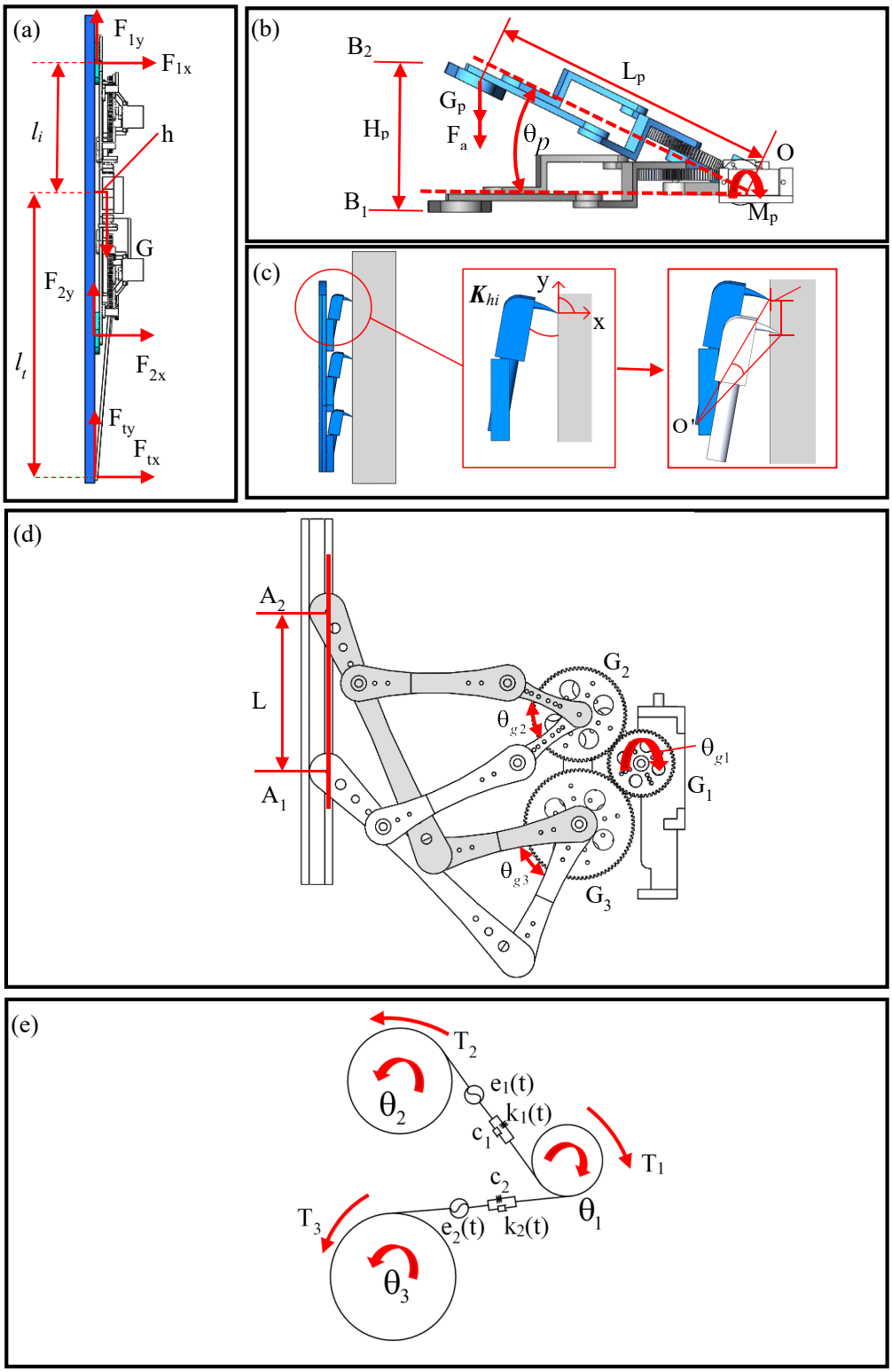

Figure 2. (**a**) Force analysis of the wall-climbing robot climbing on the wall, (**b**) force analysis of the robot's palm lifted to detach off the surface, (**c**) force analysis of the robot's palm adhere to the surface, (**d**) the motion analysis of the robot's palm for climbing, (**e**) the dynamic mechanics' mode of the transmission system.

The palm of this robot adhering to the wall is shown in Figure 2c. To investigate the adhesion force of the hooks, the stiffness of the hooks is $\boldsymbol{K}_h$, the rotation angle is defined as θ′, and the adhesion force of the hooks is

$$F_h = K_h \delta_h \tag{3}$$

Here, the $\boldsymbol{K}_h$ is the stiffness matrix and δ_h is the deflection of the hook.

$$F_h = \begin{pmatrix} F_{hx} \\ F_{hy} \\ M_{h\theta'} \end{pmatrix}, \ \delta_h = \begin{pmatrix} \Delta_{\mathrm{x}} \\ \Delta_{\mathrm{y}} \\ \Delta_{\theta'} \end{pmatrix} \tag{4}$$

Here, the $\boldsymbol{F_{hx}}$ is the force of the wall on the hook in the x direction, the $\boldsymbol{F_{hy}}$ is the force in direction y, and $\boldsymbol{M}_{h\theta'}$ is the momentum of the hook. The Δ_{x}, Δ_{y}, and $\Delta_{\theta'}$ are the deflection of the hook on the wall in x, y, and bend directions.

The servos provided the torque to drive gear 1 (G1); in turn, gear 2 and gear 3 were driven. Meanwhile, link 1 and link 4 were fixed on the gears. They were driven by gear 2 and gear 3 for stretching to crawl on the wall. Figure 2d represents the two positions of the robot's palm driven by a servo through the five-link mechanism (A1, A2). The end of the link moved to the symmetry position (A1–A2) to keep the robot's palm moving in a straight line. While the robot's palm stretched to position A2, gear 1, gear 2, and gear 3 turned θ_{g1}, θ_{g2} and θ_{g3}, respectively. During this situation, the linear velocity of the gears was kept the same:

$$V_1(\mathrm{t}) = V_2(t) = \mathrm{V}_3(t) \tag{5}$$

hence,

$$\omega_1(\mathrm{t}) r_1 = \omega_2(\mathrm{t}) r_2 = \omega_3(\mathrm{t}) r_3 \tag{6}$$

$$\theta_{\mathrm{g}1}(\mathrm{t}) = \omega t \tag{7}$$

$$\theta_{\mathrm{g}1}(\mathrm{t}) d_1 = \theta_{\mathrm{g}2}(\mathrm{t}) d_2 = \theta_{\mathrm{g}3}(\mathrm{t}) d_3 \tag{8}$$

$$d = mz \tag{9}$$

$$\theta_{\mathrm{g}1}(\mathrm{t}) z_1 = \theta_{\mathrm{g}2}(\mathrm{t}) z_2 = \theta_{\mathrm{g}3}(\mathrm{t}) z_3 \tag{10}$$

Here, V_1, V_2, and V_3 are the linear velocity of the gears; ω_1, ω_2, ω_3 represent the angular velocities of the gears; d shows the pitch diameter of the gear; m is the module of the gear; z is the number of teeth; and z_1, z_2, and z_3 represent the number of teeth of the gear 1, gear 2, and gear 3, respectively. The parameters of gear 1, gear 2, and gear 3 can be obtained by Equation (10), based on the length of the links.

2.3. Kinetic Analysis

This robot had four legs for climbing on the wall. The legs were driven by the gear transmission. The gear transmission affected the stability of crawling system. Hence, the kinetic analysis of the gear transmission was so important that the relevant dynamic model was proposed. Before the model building, the following hypothesis was proposed:

1. The internal and external mesh pairs were represented by virtual spring-damping units, time-varying stiffness, and comprehensive transmission error.
2. The frictions of each meshing pair and supporting bearings could be neglected.
3. The backlashes of gear pairs were included.

Figure 2e presents the dynamic mechanics of the gear transmission system in a foot of this robot. The θ_i (I = 1, 2, 3) is the displacement of the gears, I_i (i = 1, 2, 3) represents the moment of inertia of the gear, and e_j (t), (j = 1, 2) is the comprehensive transmission error during the process of gear driving. The comprehensive transmission error e_j (t) is periodic and varies with the mesh frequency ω_j, which can be written as

$$e_j(t) = E_j \cos(\omega_j t + \varphi_j) \tag{11}$$

where E_j is the comprehensive gear meshing error amplitude and φ_j is the phase angle of the j_{th} gear pair. The $k_j(t)$, (j = 1, 2) is the time-varying mesh stiffness and can be described as

$$k_j(t) = k_{mj} + k_s \cos(\omega_j t + \varphi_{kj}) \tag{12}$$

where k_{mj} is the average amplitude, k_s is the varying amplitude of the j_{th} time-varying mesh stiffness of gear pair, φ_{kj} is the phase angle of this gear pair, c_j, (j = 1, 2) is the damping coefficient, T_1 is the driving moment, and T_2 and T_3 are the driven moments on the gear. The dynamic mechanics' function of this gear system can be written as

$$\begin{cases} I_2\ddot{\theta}_2 + c_1R_2(R_2\dot{\theta}_2 - R_1\dot{\theta}_1 - \dot{e}_1(t)) + k_1(t)R_2f(R_2\theta_2 - R_1\theta_1 - e_1(t)) = T_2 \\ I_3\ddot{\theta}_3 + c_2R_3(R_3\dot{\theta}_3 - R_1\dot{\theta}_1 - \dot{e}_2(t)) + k_2(t)R_3f(R_3\theta_3 - R_1\theta_1 - e_2(t)) = T_3 \\ I_1\ddot{\theta}_1 - c_1R_1(R_2\dot{\theta}_2 - R_1\dot{\theta}_1 - \dot{e}_1(t)) - k_1(t)R_1f(R_2\theta_2 - R_1\theta_1 - e_1(t)) \\ -c_2R_1(R_3\dot{\theta}_3 - R_1\dot{\theta}_1 - \dot{e}_2(t)) - k_2(t)R_1f(R_3\theta_3 - R_1\theta_1 - e_2(t)) = -T_1 \end{cases} \tag{13}$$

Here, R_i (i = 1, 2, 3) represents the radius of the gears. This model only included the torsional direction displacement. This gear transmission system included the gear backlash, represented by Figure 2e. The displacement function $f(X_i)$ that included the gear backlash can be expressed as

$$f(X_j) = \begin{cases} X_j - b & X_j > \mathrm{b} \\ 0 & |X_j| \le \mathrm{b} \\ X_j + b & X_j < -\mathrm{b} \end{cases} \tag{14}$$

In order to eliminate the rigid body movement, the relative displacements of the gear pair were proposed as X_j (j = 1, 2). These can be obtained as

$$\begin{cases} X_1 = R_2\theta_2 - R_1\theta_1 - e_1(t) \\ X_2 = R_3\theta_3 - R_1\theta_1 - e_2(t) \end{cases} \tag{15}$$

Hence, the function can be written

$$\begin{cases} \ddot{X}_1 + c_1R_2^2/I_2\dot{X}_1 + c_1R_1^2/I_1\dot{X}_1 + c_2R_1^2/I_1\dot{X}_2 + k_1(t)R_2^2/I_2f(X_1) + k_1(t)R_1^2/I_1f(X_1) \\ \qquad +k_2(t)R_1^2/I_1f(X_2) = -\ddot{e}_1(t) + R_2T_2/I_2 + R_1T_1/I_1 \\ \ddot{X}_2 + c_2R_3^2/I_3\dot{X}_2 + c_2R_1^2/I_1\dot{X}_2 + c_1R_1^2/I_1\dot{X}_1 + k_2(t)R_3^2/I_3f(X_2) + k_2(t)R_1^2/I_1f(X_2) \\ \qquad +k_1(t)R_1^2/I_1f(X_1) = -\ddot{e}_2(t) + R_1T_1/I_1 + R_3T_3/I_3 \end{cases} \tag{16}$$

The dimensionless process was used to solve this function to obtain the vibration placement. The normal dimension b_c is

$$b_c = b/\,\overline{b} \tag{17}$$

where the $\overline{b}$ is dimension value. The characteristic frequency ω_{n} can be expressed as

$$\omega_{\mathrm{n}} = \sqrt{k_{mj}/(1/m_1 + 1/m_2)} \tag{18}$$

The dimensionless treatment of displacement, velocity, and acceleration are shown as

$$\begin{cases} X_i = \overline{X}_i b_c \\ \dot{X}_i = \dot{\overline{X}}_i \omega_n b_c \\ \ddot{X}_i = \ddot{\overline{X}}_i \omega_n^2 b_c \end{cases} \tag{19}$$

The gear backlash can be expressed as

$$f(\overline{X}_j) = \begin{cases} \overline{X}_j - \overline{b} & \overline{X}_j > \overline{b} \\ 0 & |\overline{X}_j| \le \overline{b} \\ \overline{X}_j + \overline{b} & \overline{X}_j < -\overline{b} \end{cases} \tag{20}$$

The time-varying mesh stiffness and comprehensive transmission error can be presented as

$$\begin{cases} \overline{e}_j(t) = \overline{E}_j \cos(\overline{\omega}_j t + \varphi_j) \\ \overline{k}_j(t) = k_{mj} + k_s \cos(\overline{\omega}_j t + \varphi_{kj}) \end{cases} \tag{21}$$

where $\overline{\omega}_j = \omega_j/\omega_n$, $\overline{E}_j = E_j/b_c$. The function can be expressed as

$$\begin{cases} \omega_n^2 b_c \ddot{\overline{X}}_1 + \omega_n b_c c_1 R_2^2/I_2 \dot{\overline{X}}_1 + \omega_n b_c c_1 R_1^2/I_1 \dot{\overline{X}}_1 + \omega_n b_c c_2 R_1^2 I_2 \dot{\overline{X}}_2 + b_c k_1(t) R_2^2/I_2 f(\overline{X}_1) \\ \quad + b_c k_1(t) R_1^2/I_1 f(\overline{X}_1) + b_c k_2(t) R_1^2/I_1 f(\overline{X}_2) = -\ddot{\overline{e}}_1(t) + R_2 T_2/I_2 + R_1 T_1/I_1 \\ \omega_n^2 b_c \ddot{\overline{X}}_2 + \omega_n b_c c_2 R_3^2/I_3 \dot{\overline{X}}_2 + \omega_n b_c c_2 R_1^2/I_1 \dot{\overline{X}}_2 + \omega_n b_c c_1 R_1^2 I_3 \dot{\overline{X}}_1 + b_c k_2(t) R_3^2/I_3 f(\overline{X}_2) \\ \quad + b_c k_2(t) R_1^2/I_1 f(\overline{X}_2) + b_c k_1(t) R_1^2/I_1 f(\overline{X}_1) = -\dot{\overline{e}}_2(t) + R_1 T_1/I_1 + R_3 T_3/I_3 \end{cases} \tag{22}$$

$$\begin{cases} \ddot{\overline{X}}_1 = -\ddot{\overline{e}}_1(t) + T_2/(R_2 \omega_n^2 b_c m_2) + T_1/(R_1 \omega_n^2 b_c m_1) - (c_1/(\omega_n m_2) - c_1/(\omega_n m_1))\dot{\overline{X}}_1 \\ \quad -c_2/(\omega_n m_1)\dot{\overline{X}}_2 - k_1(t)(1/(\omega_n^2 m_2) - 1/(\omega_n^2 m_1)) f(\overline{X}_1) - k_2(t)/(\omega_n^2 m_1) f(\overline{X}_2) \\ \ddot{\overline{X}}_2 = -\ddot{\overline{e}}_2(t) + T_1/(R_1 \omega_n^2 b_c m_1) + T_3/(R_3 \omega_n^2 b_c m_3) - (c_2/(\omega_n m_3) - c_2/(\omega_n m_1))\dot{\overline{X}}_2 \\ \quad -c_1/(m_1 \omega_n)\dot{\overline{X}}_1 - k_2(t)(1/(\omega_n^2 m_3) - 1/(\omega_n^2 m_1)) f(\overline{X}_2) - k_1(t)/(\omega_n^2 m_1) f(\overline{X}_1) \end{cases} \tag{23}$$

This can be written as

$$M\ddot{\overline{X}} + C\dot{\overline{X}} + K\overline{X} = \overline{F} \tag{24}$$

where

$$M = \begin{pmatrix} 1 & 0 \\ 0 & 1 \end{pmatrix}, \ \overline{X} = \begin{pmatrix} \overline{X}_1 \\ \overline{X}_2 \end{pmatrix} \tag{25}$$

$$C = \begin{pmatrix} -c_1/\omega_n(1/m_2 + 1/m_1) & -c_2/(\omega_n m_1) \\ -c_1/(m_1 \omega_n) & -c_2/\omega_n(1/m_3 + 1/m_1) \end{pmatrix} \tag{26}$$

$$K = \begin{pmatrix} -k_1(t)(1/m_2 + 1/m_1)/\omega_n^2 & -k_2(t)/(\omega_n^2 m_1) \\ -k_1(t)/(m_1 \omega_n^2) & -k_2(t)(1/m_3 + 1/m_1)/\omega_n^2 \end{pmatrix} \tag{27}$$

$$F = \begin{pmatrix} T_2/(R_2 \omega_n^2 b_c m_2) + T_1/(\mathrm{R}_1 \omega_n^2 b_c m_1) - \ddot{\overline{e}}_1(t) \\ T_3/(R_3 \omega_n^2 b_c m_3) + T_1/(\mathrm{R}_1 \omega_n^2 b_c m_1) - \ddot{e}_2(t) \end{pmatrix} \tag{28}$$

Equation (24) of the gear transmission system can be solved by the Runge–Kutta method.

The parameters of the whole system are shown in Table 1.

Table 1. The parameters of the gears.

Gear	Teeth	Module	Pressure Angle (°)	Width (mm)	Mass (g)
Gear 1	50	0.5	20	5	1.96
Gear 2	71	0.5	20	5	4.17
Gear 3	83	0.5	20	5	6

The relative displacements of gear 1, gear 2, and gear 3 were obtained from Equation (24) by the Runge–Kutta method. The results are shown in Figure 3. Figure 3a represents the dimensionless relative displacements of gear 1 and gear 2; these ranged between –0.1902~0.1905. Figure 3b represents the dimensionless relative displacements of gear 1 and gear 3; these ranged between −0.2001~0.20. The dimensionless relative displacements of gear 1 and gear 2 were larger than gear 1 and gear 3. The deformations of gear 1 and gear 3 were larger than that of gear 1 and gear 2. Therefore, the vibration displacement of gear 3 was larger than the gear 2. To investigate the stability of these three gears, the phase images and Poincare maps are presented in Figure 4. From Figure 4, the phase images of gear 1 with gear 2 was a single ellipse and the gear 1 meshed with gear 2 was a stability state in this situation. The cycle time was doubled in this gear transmission state as the Poincare map had two red points. The gear 1 meshed with gear 3 had the same cyclic motion state, but the vibration amplitude of gear 1 with gear 3 was larger than the gear 1 with gear 2.

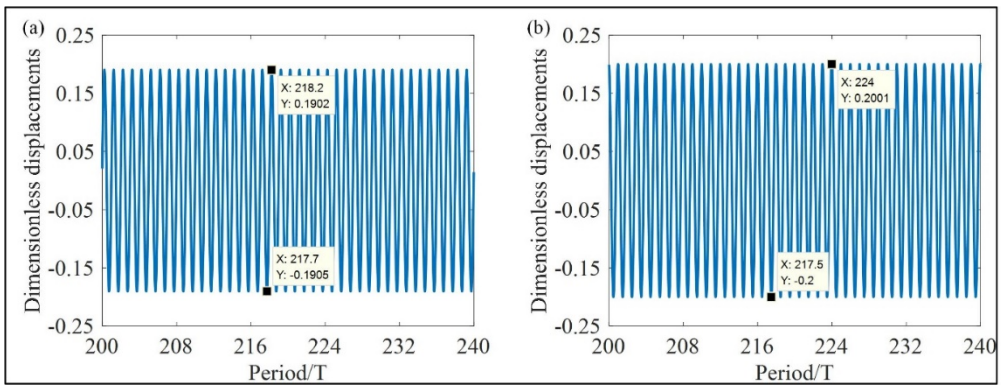

Figure 3. (**a**) The dimensionless relative displacement of the gear 1 and gear2, (**b**) the dimensionless relative displacement of the gear 1 and gear 3.

In order to investigate the effect of the angle on the adherence force, the theoretical model of this claw when climbing the rough surface is shown in Figure 5d. In this figure, two small circles represent the two tips of the spine, which contacts the rough surface. The radius of the two smaller circles is r. The bigger circle is the particle on the rough surface, whose radius is R. These two small circles are tangent to the big circle. They express the cicada's claw adherence to the rough surface. The angle between these two circles is γ, which represents the angle of the hooks on the end of the leg. The contract angle between the cicada's claw and the rough surface is α_i (α_1, α_2).

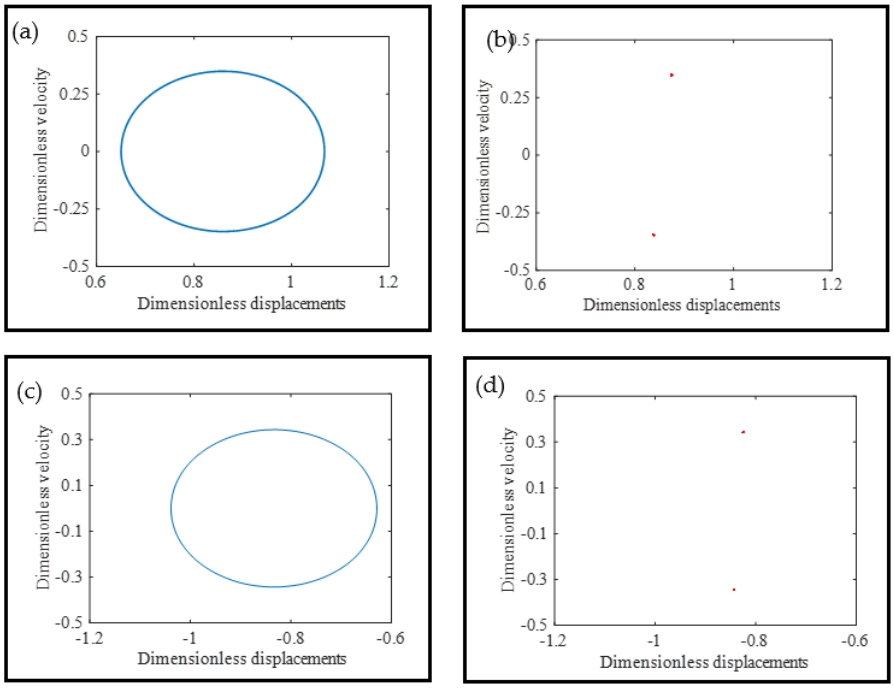

Figure 4. (**a**) The phase images of the gear 1 and gear 2. (**b**) The Poincare maps of the gear 1 and gear 2. (**c**) The phase images of the gear 1 and gear 3. (**d**) The Poincare maps of the gear 1 and gear 3.

2.4. Adhesion Part Analysis

Figure 5a is the cicada, which has the ability to climb trees by using its biometry claws. Figure 5b represents the detailed image of the cicada's claw. From this image, we can see a special bifurcated spine on the end of the claw. The cicada can climb trees by using these bifurcated spines. This paper investigated the use of bifurcated spines in a proposed wall-climbing robot for climbing on rough surfaces. This paper presents a bionic spine design that was inspired by this special hook with an angle, as shown in Figure 5c.

The contact angle α is

$$\alpha = arcsin(\frac{r+R-h}{r+R}) = arcsin(1-\frac{h}{r+R}) \tag{29}$$

Figure 5e expresses the equivalent force diagram of the bionic hook adhering to the rough surface. The load distribution force angle is β (β_1, β_2), the height of the particle is h, f (f_1, f_2) is the friction force between hook and surface, F (F_1, F_2) is the comprehensive capsizing force of the hook by the wall and the weight of the hook, and N (N_1, N_2) is the support force on the hook by the wall. To adhere to the protruding particles, the mechanics must satisfy:

$$\begin{cases} \sum\limits_{i=1}^{n} f_i sin(\gamma_i/2) = \sum\limits_{i=1}^{n} \mu_i N_i cos(\gamma_i/2) \\ \qquad\qquad = \sum\limits_{i=1}^{n} F_i sin(\alpha_i+\beta_i) \\ \sum\limits_{i=1}^{n} N_i = \sum\limits_{i=1}^{n} F_i cos(\alpha_i+\beta_i) \end{cases} \tag{30}$$

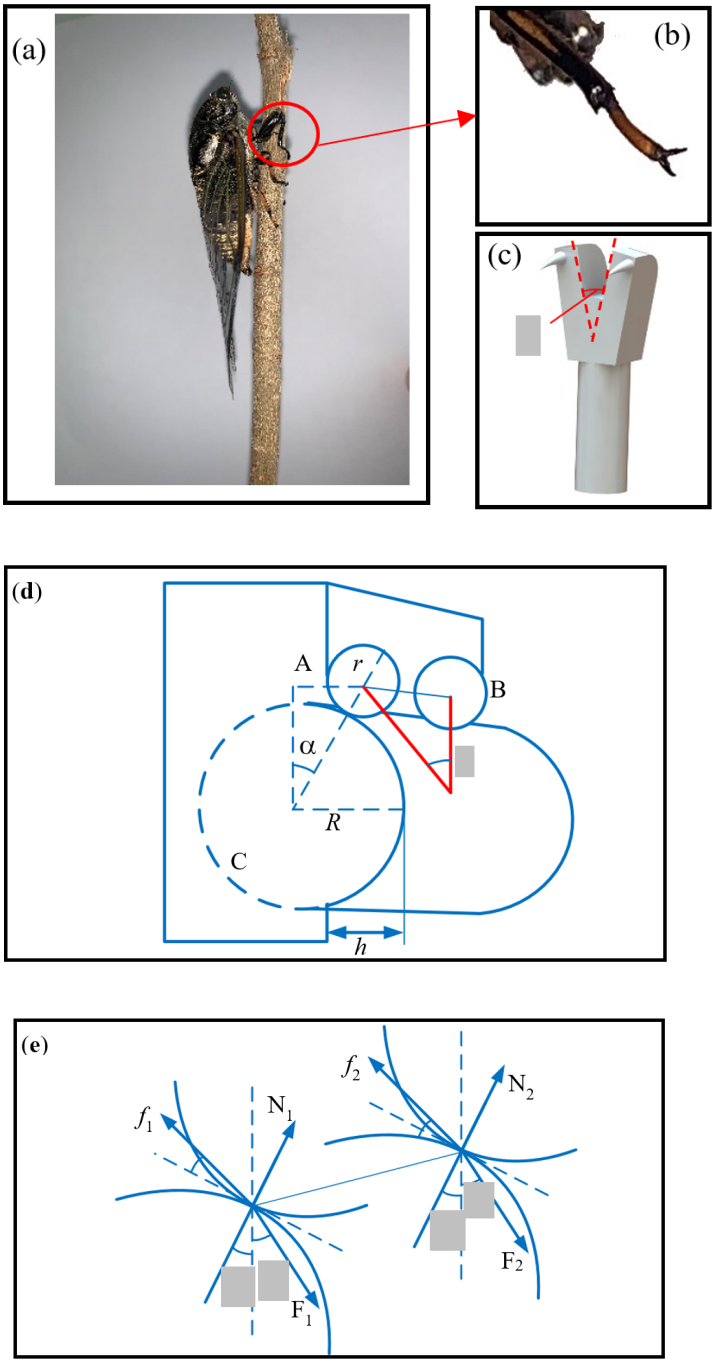

Figure 5. (**a**) A cicada on the branch of the tree, (**b**) a leg of a cicada, (**c**) the bionic bifurcated spines inspired by the cicada's claws, (**d**) equivalent force diagram of the bionic hook. (**e**) The equivalent force diagram of the bionic hook adhering to the rough surface.

In terms of a single hook,

$$\beta < arctan(2\mu cos(\gamma/2)) - \alpha \tag{31}$$

Here, μ is the friction coefficient between the hook and the surface.
Integrating with Equations (29)–(31), β is written as

$$\beta < arctan(2\mu cos(\gamma/2)) - arcsin(1 - \frac{h}{r+R}) \tag{32}$$

The hooks' adherence on the rough surface must satisfy the condition that β is greater than zero. This means that α is limited and is less than $arctan(\mu cos(\gamma/2))$, from Equation (31). Here, α is defined by the diameter and the height of the particle and α is the angle of the hook to change the adhere characteristics of the hooks. These parameters are investigated by the following figures. Figure 6a represents the relations of the pressure angle (α) and the load distribution angle (β) with various hooks' angles γ. In this figure, the load distribution angle (β) decreases as the hook angles γ decrease. It means that decreasing the hook angles γ improves the adherence property. The relation between the size of hooks and the particles on the contact surface is provided in Figure 6b. In this figure, the smaller the radius of the hooks' angle, the bigger the load distribution angle (β), as the height and the radius of the particles remain unchanged. Hence, decreasing the size of the hook's end can develop the adherence property.

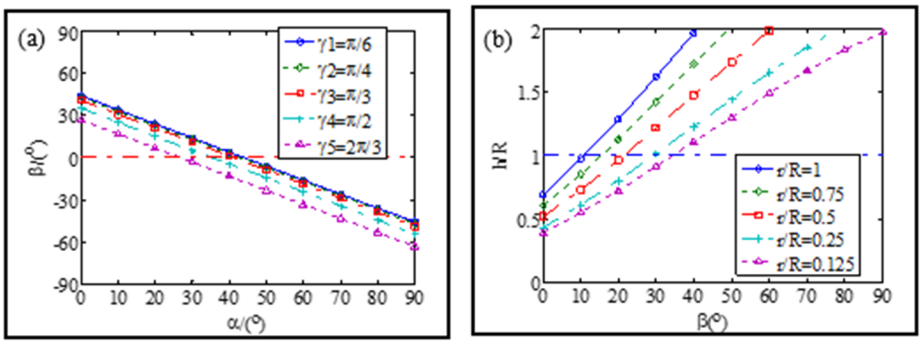

Figure 6. (**a**) The relation of the pressure angle (α) and the load distribution angle (β) with various hook angles (γ), (**b**) the relation of the load distribution load angle and the particles' sizes on the contact surface with different sizes of hooks.

2.5. Adhesion Part Analysis

As shown in Figure 7, the tangential adhesive force of the various hook angles of the bionic claws were examined on the adhesive test platform. A rough surface was put on the platform for testing.

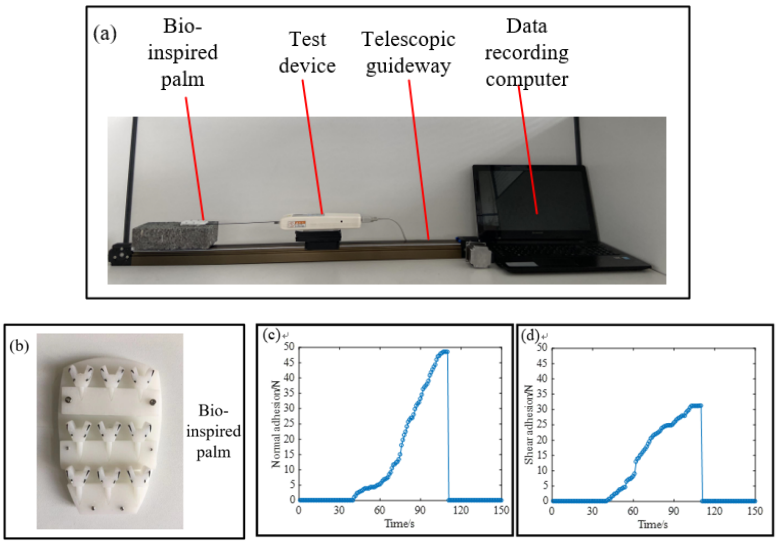

Figure 7. The adhesion force of the bionic palm. (**a**) A measuring platform to measure the adhere force. (**b**) The bionic palm with various bionic spines. (**c**) The normal adhesion force of this bionic palm. (**d**) The shear adhesion force of this bionic palm.

Figure 7a represents the testing set for adhesive materials. The testing device and the telescopic guideway are on the right; the testing materials are on the left. The adherence

palm that was bio-inspired by the cicada (the hook angle is 60°) was put on the brick that was fixed on the platform. The testing device was a force test set that could record the data during the testing. The testing device was fixed on the telescopic guideway with a motor pulling the bionic palm and recording the force data. The preload of the robot's palm was 0.12 N on the wall during climbing. Hence, the preload on the adherence palm was also 0.12 N during the measuring. Figure 7c,d shows the normal adhesion force and the shear adhesion force of the bionic palm (Figure 7b), respectively. The maximum of the normal adhesion force reached 48.7 N, and the maximum of the shear adhesion force reached 31.5 N.

To adhere to the smooth surface, we borrowed the adhesion characteristics of a gecko's toes with numerous bristles' arrays. Figure 8a is a gecko from an animal breeding base. Figure 8b is the gecko's toe and the Figure 8c is the scanning electron microscope image of the gecko's toe. From Figure 8c, there are numerous bristles' arrays on the toe to help the gecko adhere to the wall for climbing.

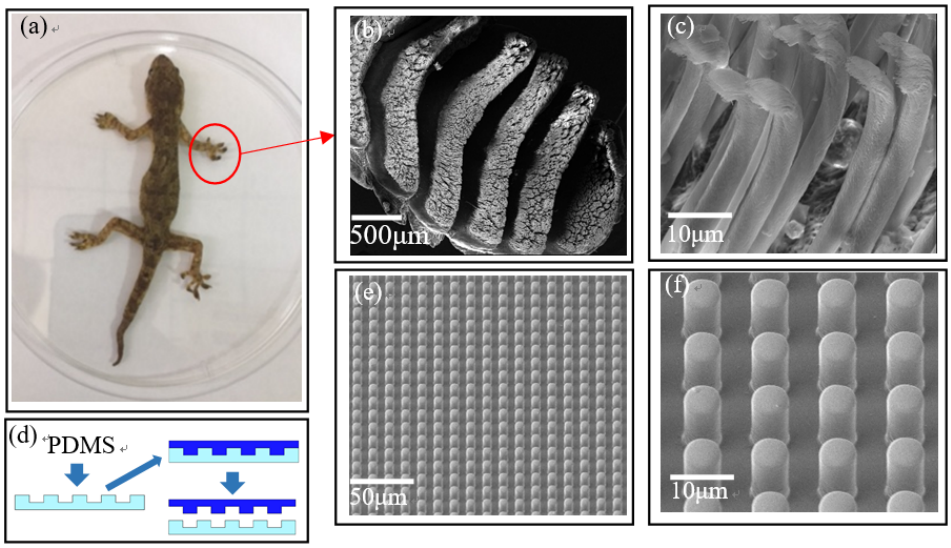

Figure 8. (**a**) The photo of the gecko, (**b**) scanning electron micrograph of a gecko's toe, (**c**) the extended scanning electron micrograph of a gecko's toe. (**d**) The PDMS was taken from the silicon plate to obtain an adhesion sheet. (**e**) The gecko-inspired setae array, (**f**) the extended image of the gecko-inspired setae array.

Furthermore, the photolithography technology was used to make the bionic bristles' array (Figure 8d). This bionic bristles' array is made of PDMS (Polydimethylsiloxane), as shown in Figure 8e,f. The diameter of the bristle was 7 μm and the height was 10 μm. After the adhesive sheet was manufactured, a 40-mm × 50-mm rectangle sheet was cut for measuring. The result is presented in Figure 9.

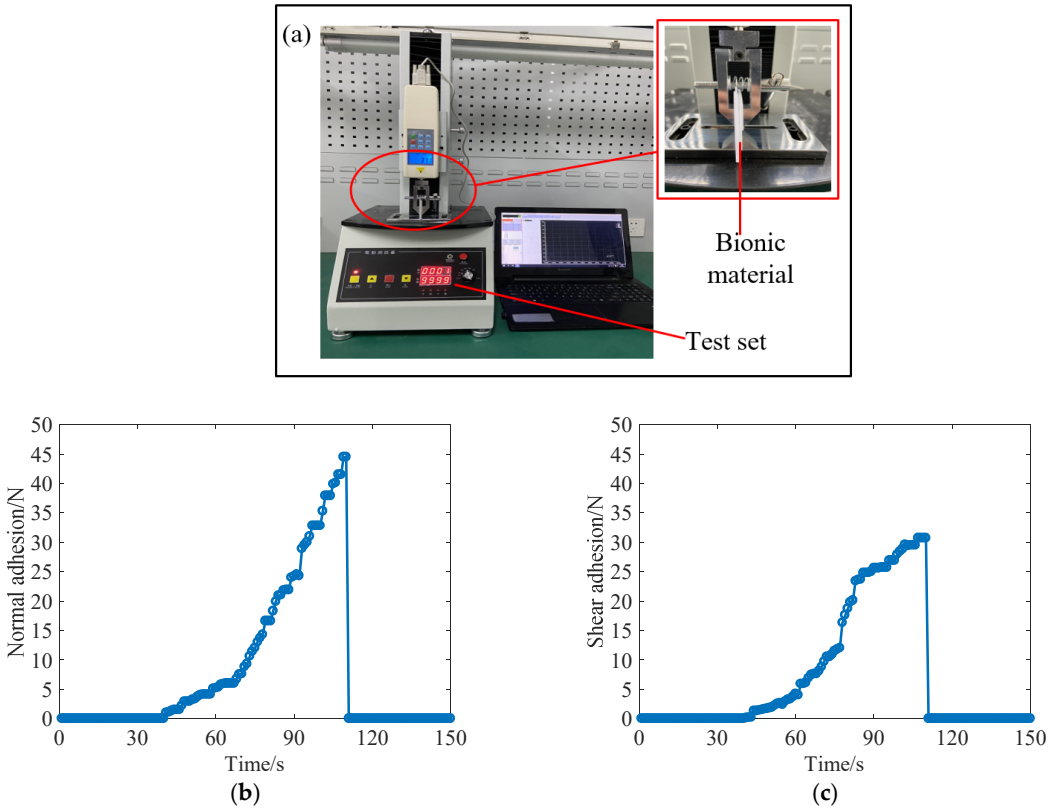

Figure 9. The test set to measure the adherence force. (**a**) The test set for measuring the adherence force of the bio-inspired materials. (**b**) The test set to measure the normal force of the adhesive materials. (**c**) The shearing force of the adhesive materials without preload.

The adherence materials (40 mm × 50 mm) that were put on the glass fixed on the platform, as shown in Figure 9a–c, showed normal adherence force and shear adherence force, respectively. The maximum of the normal adherence materials reached 44.5 N, and the maximum of the shear adherence force reached 30.7 N. This rectangle sheet was manufactured for the bionic robot to adhere to the smooth surface.

3. Locomotion of the Robot

The proposed robot climbed on the wall with stability by an efficient locomotion gait, as shown in Figure 10. This climbing strategy was divided into six parts by the servos to realize the robot's legs lifting and stretching. In each period, the foot (I) and the foot (IV) moved in sync, and the foot (II) and foot (III) moved in sync. The foot with blue color means that the foot was in the attaching status, while the white color indicates it was in the detaching status. However, each foot was in two positions when the robot climbed the wall: One was at the stretching position and the other was at the contraction position. The stretching position was the point of the robot's foot after the stretching was completed and the contraction position was the point of the robot's foot after contracting was completed.

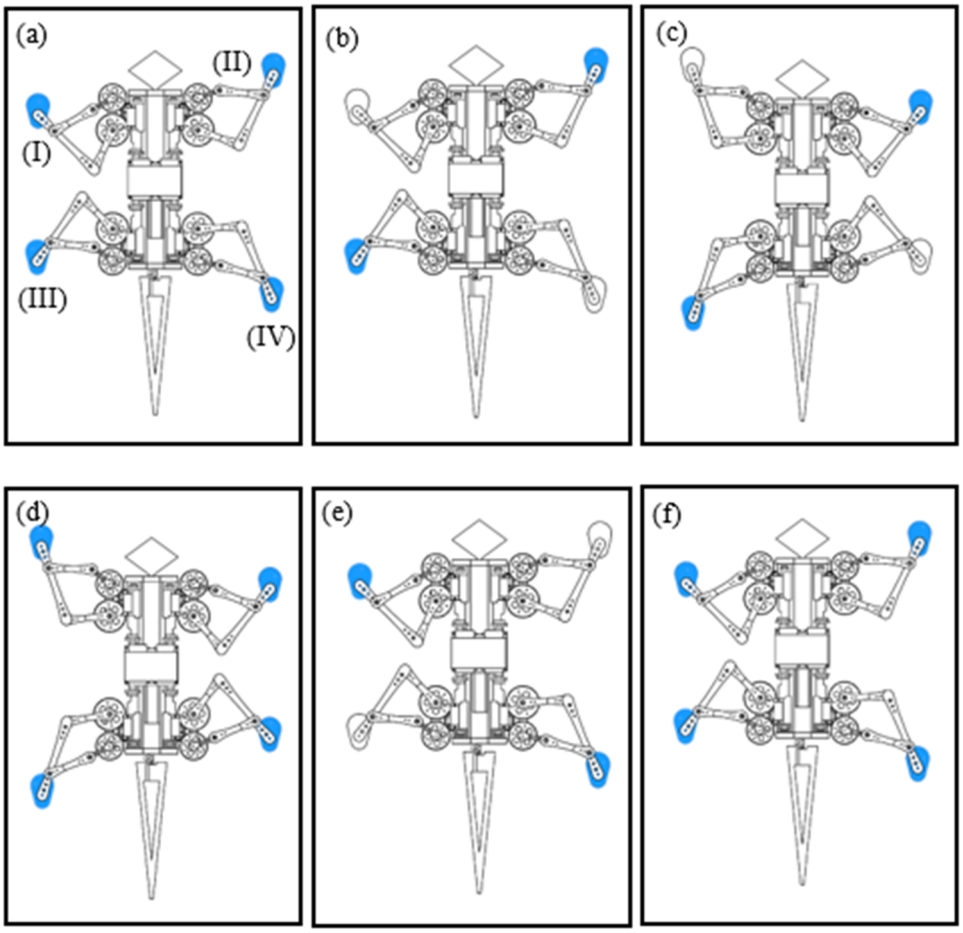

Figure 10. (**a**) The first step in a single cycle, (**b**) the second step in a single cycle, (**c**) the third step in a single cycle, (**d**) the fourth step in a single cycle, (**e**) the fifth step in a single cycle, and (**f**) the sixth step in a single cycle.

In the first step (Figure 10a), the four feet of the robot all attached to the surface. The foot (I) and the foot (IV) were at the contraction position and the foot (II) and the foot (III) were at the stretching position.

In the second step (Figure 10b), the foot (II) and the foot (III) remained attached at the above position. Then, the foot (I) and the foot (IV) lifted away from the surface by the servos.

In the third step (Figure 10c), the foot (II) and the foot (III) were attached at the above position and the servo drove the gear transmission system to elevate the body. Meanwhile, the servo drove the gear transmission system to stretch the foot (I) and the foot (IV).

In the fourth step (Figure 10d), the foot (II) and the foot (III) were attached at the above position. The servo drove the foot (I) and the foot (IV) down to attach to the surface. The four feet were all attached on the surface in this step.

In the fifth step (Figure 10e), the servo drove the gear transmission to the control foot (I) and the foot (IV) to the contraction position for elevating the body. At the same time, the servo uplifted the foot (II) and the foot (III) and detached from the surface to the stretching position.

In the last step (Figure 10f), the foot (I) and the foot (IV) were kept attached at the above contraction position. The servo drove the foot (II) and the foot (III) down and attached them to the surface.

4. Experiment

The dimensions of the gear transmission robot prototype are shown in Table 2. The components of this bionic, wall-climbing robot were made from resin by a 3D printing

method. The manufactured parts were assembled with the adhesion hooks (Figure 7b) and the adhesion materials (Figure 8e) to complete the climbing experiment as follow.

Table 2. The dimensions of the robot prototype.

Design Parameters	Values
Length of robot (with tail)	474 mm
Width of body (include the legs)	330 mm
Mass of robot	360 g
Size of pad	40 mm × 50 mm
One-step duration	0.15 s

The locomotion of this robot climbing the vertical cloth, stones, and glass walls in a cycle is shown in Figures 11–13, respectively. This robot climbed from the dotted line to the real line. The laser position device recorded the displacement of the robot in a cycle, as shown in Figure 14. The robot climbing 90.10 mm on the horizontal cloth surface and 79.7mm on the vertical cloth surface is presented in Figure 14b (i) and (ii). The locomotion time of each step was 0.15 s. Then, the six steps took 0.9 s in a cycle. The theoretical speed of the robot was 11.34 cm/s, and the experimental were 10.01 cm/s and 8.86 cm/s on the horizontal and vertical wall, respectively. The theoretical speed of the robot when climbing walls was higher than the experimental results. The difference between theory and experimental was due to the robot assembling error. The displacements of the robot in a cycle on the stones and glass are shown in Figure 14b (iii) and (iv), respectively. The robot climbed 82.29 mm on the vertical stone surface and 84.02 mm on the vertical glass surface. The climbing speeds of the robot on the stone wall and glass wall were 9.14 cm/s and 9.34 cm/s, as shown in Table 3, respectively. When the wall-climbing robot climbed the cloth surface, the cloth surface was slightly damaged, and when it climbed the stone surface, the hook stabbing was slightly damaged. The different climbing speeds of the robot may have been due to the surface materials. The robot can adapt to different surfaces by changing the adhesion materials. Research on multiple series of materials can broaden the scope of application of robots.

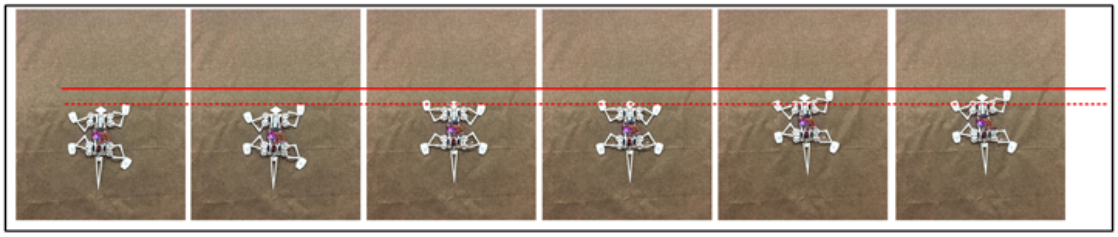

Figure 11. Experiment of the locomotion of the bionic robot climbing on the cloth surface in cycle.

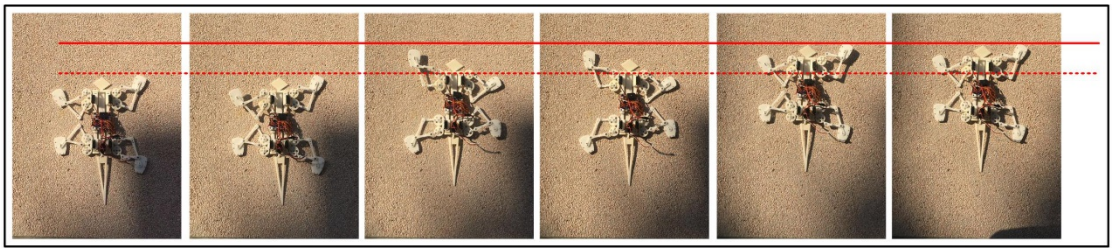

Figure 12. Experiment of the locomotion of the bionic robot climbing on the stone surface in cycle.

Figure 13. Experiment of the locomotion of the bionic robot climbing on the glass surface in cycle.

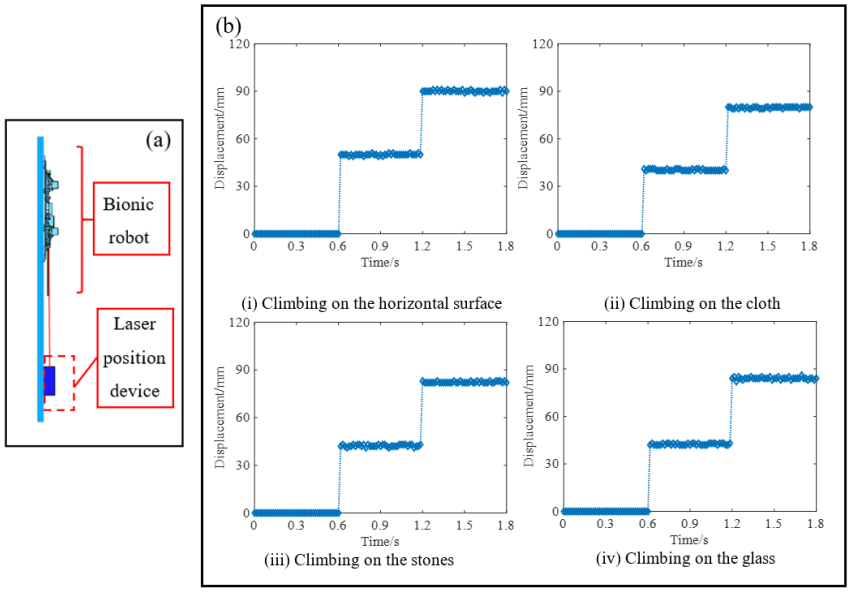

Figure 14. (**a**) Experiment of the locomotion speed of the bionic robot by the laser position device, (**b**) the displacement profile of the robot.

Table 3. The speed of the robot prototype.

Climbing Surfaces	Velocity (Vertical)
Cloth	8.86 cm/s
Stones	9.14 cm/s
Glass	9.34 cm/s

Table 4 lists the speed parameters of various wall-climbing robot. Compared with these climbing robots (Waalbot II, Stickbot, Spinybot II, as shown in Table 4), it is rarely adapted to multi-surfaces. Waalbot II and Stickbot were designed for smooth surfaces, while Spinybot II was designed for rough surfaces. Few robots are designed to climb multiple walls. This paper's robot climbed on the smooth and rough surfaces. The speed of this robot was 8.86 cm/s, 9.14 cm/s, and 9.34 cm/s on the cloth, stones, and glass. Compared to these climbing robots in Table 4, this paper's robot expands the scope of application and performs well in terms of climbing speed.

Table 4. The comparison of the robots.

Wall-Climbing Robot	Climbing Surfaces	Velocity (Vertical)	Climbing on Multi-Surfaces
Waalbot II [10]	Glass	5 cm/s	No
Stickbot [11]	Glass	4 cm/s	No
Spinybot II [19]	Stones	4 cm/s	No

5. Conclusions

In this paper, a wall-climbing robot that can adhere to rough and smooth surfaces inspired by cicadas and geckos was proposed. A new type of climbing structure was designed with a gear-link transmission to improve the stability of the robot when climbing a wall. This robot had a special angle spine adhesion palm for the rough surface that was inspired by the cicada. Meanwhile, the robot palm used adhesion materials, inspired by the gecko, for smooth surfaces. This palm design allowed the robot to effectively adhere to a wall. The robot was experimentally evaluated on vertical rough and smooth surfaces. It reached a speed of 8.86 cm/s on the cloth surface, 9.14 cm/s on the stone surface, and 9.34 cm/s on the glass surface. Compared to other robots, this robot had a good performance. This type of robot provided an idea for the research of wall-climbing robots that deal with a variety of wall surfaces. This robot has practical applications, including inspecting rough and smooth surfaces.

Author Contributions: Conceptualization, D.K.; writing—original draft preparation, S.B.; validation, F.X.; formal analysis, Y.W.; All authors have read and agreed to the published version of the manuscript.

Funding: This research received no external funding.

Institutional Review Board Statement: Ethical review and approval were waived for this study, due to this paper don't involve ethical issue.

Informed Consent Statement: Not applicable.

Data Availability Statement: The study did not involve important data.

Conflicts of Interest: The authors declare no conflict of interest.

References

1. Maderson, P.F. Keratinized epidermal derivatives as an aid to climbing in gekkonid lizards. *Nature* **1964**, *203*, 780–781. [CrossRef]
2. Hiller, U. Untersuchungen zum Feinbau und zur Funktion der Haftborsten von Reptilien. *Z. Morphol. Tiere* **1968**, *62*, 307–362. [CrossRef]

3. Russell, A.P. A contribution to the functional morphology of the foot of the tokay, Gekko gecko (Reptilia, Gekkonidae). *J. Zool.* **2009**, *176*, 437–476. [CrossRef]
4. Autumn, K.; Liang, Y.A.; Hsieh, S.T.; Zesch, W.; Chan, W.P.; Kenny, T.W.; Fearing, R.; Full, R.J. Adhesive force of a single gecko foot-hair. *Nature* **2000**, *405*, 681–685. [CrossRef] [PubMed]
5. Autumn, K.; Sitti, M.; Liang, Y.A.; Peattie, A.M.; Hansen, W.R.; Sponberg, S.; Kenny, T.W.; Fearing, R.; Israelachvili, J.N.; Full, R.J. Evidence for van der Waals adhesion in gecko setae. *Proc. Natl. Acad. Sci. USA* **2002**, *99*, 12252–12256. [CrossRef] [PubMed]
6. Unver, O.; Uneri, A.; Aydemir, A.; Sitti, M. Geckobot: A gecko inspired climbing robot using elastomer adhesives. In Proceedings of the IEEE International Conference on Robotics and Automation, Orlando, FL, USA, 15–19 May 2006; pp. 2329–2335.
7. Carlo, M.; Metin, S. A Biomimetic Climbing Robot Based on the Gecko. *J. Bionics Eng.* **2006**, *3*, 115–125.
8. Murphy, M.P.; Aksak, B.; Sitti, M. Gecko-Inspired Directional and Controllable Adhesion. *Small* **2009**, *5*, 170–175. [CrossRef] [PubMed]
9. Aksak, B.; Murphy, M.P.; Sitti, M. Gecko Inspired Micro-Fibrillar Adhesives for Wall-climbing Robots on Micro/Nanoscale Rough Surfaces. In Proceedings of the IEEE International Conference on Robotics & Automation, Pasadena, CA, USA, 19–23 May 2008; pp. 3058–3063.
10. Murphy, M.P.; Kute, C.; Menguc, Y.; Sitti, M. Waalbot II: Adhesion Recovery and Improved Performance of a Climbing Robot, using Fibrillar Adhesives. *Int. J. Robot. Res.* **2011**, *30*, 118–133. [CrossRef]
11. Kim, S.; Spenko, M.; Trujillo, S.; Heyneman, B.; Santos, D.; Cutkosky, M.R. Smooth vertical surface climbing with directional adhesion. *IEEE Trans. Robot.* **2008**, *1*, 65–74.
12. Santos, D.; Heyneman, B.; Kim, S.; Esparza, N.; Cutkosky, M.R. Gecko-inspired climbing behaviors on vertical and overhanging surfaces. In Proceedings of the International Conference on Robotics & Automation, IEEE, Pasadena, CA, USA, 19–23 May 2008; p. 1125.
13. Asbeck, A.; Dastoor, S.; Parness, A.; Fullerton, L.; Esparza, N.; Soto, D.; Heyneman, B.; Cutkosky, M.R. Climbing rough vertical surfaces with hierarchical directional adhesion. In Proceedings of the IEEE International Conference on Robotics and Automation, Kobe, Japan, 12–17 May 2009; pp. 2675–2681.
14. Hawkes, E.W.; Ulmen, J.; Esparza, N.; Esparza, N.; Cutkosky, M.R. Scaling walls: Applying dry adhesives to the real world. In Proceedings of the International Conference on Intelligent Robots and Systems, San Francisco, CA, USA, 25–30 September 2011; pp. 5100–5106.
15. Yu, Z.W.; Wang, Z.Y.; Liu, R.; Wang, P.; Dai, Z.D. Stable gait planning for a gecko-inspired robot to climb on vertical surface. In Proceedings of the International Conference on Mechatronics and Automation, Takamatsu, Japan, 4–7 August 2013; pp. 307–311.
16. Wu, X.; Wang, D.P.; Zhao, A.W.; Li, D.; Mei, T. A Wall-Climbing Robot with Biomimetic Adhesive Pedrail. In *Advanced Mechatronics and MEMS Devices*; Springer: New York, NY, USA, 2013; Volume 23, pp. 179–191.
17. Zhang, Y.J.; Wu, Y.X.; Liu, Y.W.; Hu, C.Y.; Sun, S.M.; Mei, T. Bionic Design of the Body of Tank-like Climbing Robot. In Proceedings of the International Conference on Mechatronics and Automation, Chengdu, China, 5–8 August 2012; pp. 2287–2291.
18. Dai, Z.D.; Gorb, S.N.; Schwarz, U. Roughness-dependent friction force of the tarsal claw system in the beetle Pachnoda marginata. *J. Exp. Biol.* **2002**, *205*, 2479–2488. [CrossRef] [PubMed]
19. Kim, S.; Asbeck, A.T.; Cutkosky, M.R.; Provancher, W.R. SpinybotII: Climbing Hard Walls with Compliant Microspines. In Proceedings of the 12th International Conference on, Seattle, WA, USA, 18–20 July 2005; pp. 601–606.
20. Asbeck, A.T.; Kim, S.; Cutkosky, M.R.; Provancher, W.; Lanzetta, M. Scaling Hard Vertical Surfaces with Compliant Microspine Arrays. *Int. J. Robot. Res.* **2006**, *25*, 1165–1179. [CrossRef]
21. Alan, A.T.; Kim, S.; McClung, A.; Parness, A.; Cutkosky, M.R. Climbing walls with microspines. In Proceedings of the International Conference on Robotics & Automation, Florida, IL, USA, 15–19 January 2006; pp. 4315–4317.
22. Saunders, A.; Goldman, D.; Full, R.J.; Buehler, M. The rise climbing robot: Body and leg design. *Def. Secur. Symp.* **2006**, *6230*, 1–13.
23. Spenko, M.J.; Haynes, G.C.; Saunders, J.A.; Cutkosky, M.R.; Rizzi, A.; Rizzi, A.A.; Full, R.J.; Koditschek, D.E. Biologically inspired climbing with a hexapedal robot. *J. Field Robot.* **2008**, *25*, 223–242. [CrossRef]
24. Haynes, G.C.; Khripin, A.; Lynch, G.; Amory, J.; Saunders, A.; Rizzi, A.A.; Koditschek, D.E. Rapid Pole Climbing with a Quadrupedal Robot. In Proceedings of the International Conference on Robotics and Automation, Kobe, Japan, 12–17 May 2009; pp. 12–17.
25. Goldman, D.I. Dynamics of rapid vertical climbing in cockroaches reveals a template. *J. Exp. Biol.* **2006**, *15*, 2990–3000. [CrossRef] [PubMed]
26. Clark, J.E.; Goldman, D.I.; Lin, P.C.; Lynch, G.; Chen, T.S.; Komsuoglu, H.; Full, R.J.; Koditschek, D. Design of a Bio-inspired Dynamical Vertical Climbing Robot. In Proceedings of the International Conference on Robotics: Science and Systems, Atlanta, GA, USA, 27–30 June 2007; pp. 9–16.
27. Lynch, G.A.; Clark, J.E.; Koditschek, D. A self-exciting controller for high-speed vertical running. In Proceedings of the 2009 IEEE/RSJ International Conference on Intelligent Robots and Systems, St. Louis, MO, USA, 10–15 October 2009; pp. 631–638.
28. Dickson, J.D.; Clark, J.E. The effect of sprawl angle and wall inclination on a bipedal, dynamic climbing platform. In Proceedings of the Fifteenth International Conference on Climbing and Walking Robots and the Support Technologies for Mobile Machines, Baltimore, MD, USA, 23–26 July 2012; pp. 459–466.
29. Lynch, G.A.; Clark, J.E.; Lin, P.C.; Koditschek, D.E. A bioinspired dynamical vertical climbing robot. *Int. J. Robot. Res.* **2012**, *31*, 974–996. [CrossRef]

30. Dickson, J.D.; Patel, J.; Clark, J.E. Towards maneuverability in plane with a dynamic climbing platform. In Proceedings of the International Conference on Robotics and Automation, Karlsruhe, Germany, 8–13 May 2013; pp. 1355–1361.
31. Miller, B.; Ordonez, C.; Clark, J.E. Examining the effect of rear leg specialization on dynamic climbing with SCARAB: A dynamic quadrupedal robot for locomotion on vertical and horizontal surfaces. *Exp. Robot.* **2013**, *88*, 113–126.
32. Miller, B.; Clark, J.; Darnell, A. Running in the horizontal plane with a multi-modal dynamical robot. In Proceedings of the International Conference on Robotics and Automation, Karlsruhe, Germany, 6–10 May 2013; pp. 3335–3341.
33. Wile, G.D.; Daltorio, K.A.; Diller, E.D.; Palmer, L.R.; Gorb, S.N.; Ritzmann, R.E.; Quinn, R.D. Screenbot: Walking inverted using distributed inward gripping. In Proceedings of the International Conference on Intelligent Robots and Systems, Nice, France, 22–26 September 2008; pp. 1513–1518.
34. Liu, Y.; Sun, S.; Wu, X.; Mei, T. A Wheeled Wall-Climbing Robot with Bio-Inspired Spine Mechanisms. *J. Bionic Eng.* **2015**, *12*, 17–28. [CrossRef]
35. Liu, Y.W.; Liu, S.W.; Mei, T.; Wu, X.; Li, Y. Design and Analysis of a Bio-Inspired Tracked Wall-Climbing Robot with Spines. *Robot* **2019**, *41*, 527–533.